Dynamic Current Reference Determination of Electrically Excited Synchronous Machines Based on Torque Gradients of Copper Losses

Junfei Tang, *Member, IEEE*, Bowen Jiang, *Graduate Student Member, IEEE*, Hao Chen, *Member, IEEE*, Yujing Liu, *Senior Member, IEEE*, and Stefan Lundberg, *Member, IEEE*

***Abstract*—Electrically excited synchronous machines (EESMs) have become an attractive solution to electric vehicles. The excitation of the machine can be regulated by adjusting the field current. This introduces one additional degree of control freedom. The control of the armature current in the stator and field current in the rotor is expected to not only reduce the total losses but also dynamically redistribute the load on both windings so that neither of them overheats. To realize this function, an algorithm is proposed in this study to dynamically determine the current references in EESM torque control. A cost function is introduced by placing weights on stator and rotor copper losses separately. The weights can be adjusted dynamically. The cost function is minimized by moving the current reference vector. The moving of the vector is orthogonally decomposed into a torque-related component and a cost-related component. When current or voltage limits are reached, a cancellation technique is activated to constrain the reference vector. It is shown in experimental results that expected performance is achieved in all operating conditions.**

***Index Terms*—Current reference determination, electrically excited synchronous machine (EESM), torque control.**

I. Introduction

DUE to concerns about climate change, electric vehicles (EVs) have become popular in recent years [1]. In the propulsion system of EVs, electrically excited synchronous machines (EESMs) are a promising alternative to permanent magnet synchronous machines (PMSMs) [2], [3], [4], [5], [6]. In an EESM, a field winding is employed in the rotor, and the machine is therefore free of rare-earth permanent magnets. In addition, the excitation can be controlled by adjusting the field current. Consequently, both high starting torque and wide field-weakening range can be achieved, providing the machine is designed properly [7]. Brushless excitation can be realized to avoid friction and reduce maintenance efforts [8], [9]. A unique method of sensorless rotor position estimation can be implemented in the EESM control based on ripple currents in the field winding [10], [11], [12]. This method shows an advantage of being independent from the saliency of the machine.

Compared with PMSMs, the controllable field current in an EESM rotor is an additional control freedom to the d- and q-axis armature currents in the stator. Therefore, an optimal distribution of currents among the d-axis, q-axis, and field windings to achieve a certain torque at a certain speed within current and voltage limits is to be solved. The distribution of the currents is expected to not only reduce the total losses but also prevent stator and rotor windings from overheating. In addition, the distribution should be dynamically adjustable according to the condition of the machine. For instance, when the temperature of the field winding rises towards the limit, the field current should decrease whereas the stator current should increase so that the torque is maintained and vice versa.

Studies on this topic have been pursued in previous research activities. In [13], a method is proposed to minimize the overall losses of a salient pole EESM in different working conditions including torque-boosting and field-weakening. An analytical minimization of total copper losses serves as an initial approximation, which is then followed by an offline numerical minimization based on measurement data. In [14] and [15], field current optimization strategies have been proposed by introducing a magnetic equivalent circuit model or a dynamic equivalent core loss resistance in order to improve the efficiency, including both iron core losses and copper losses. In [16] and [17], a numerical iteration algorithm based on finite element method (FEM) data is proposed. The cost function in this case is adjustable by placing different weights on stator and rotor copper losses separately. It is shown that the assignment of weights influences the distributions of stator and rotor currents in the torque-speed map effectively.

However, the methods proposed in the above-mentioned studies are off-line. This means that look-up tables in torque-speed coordinates are off-line calculated and then used in online control. In contrast to the off-line approach, an online copper-loss-minimizing torque control method is proposed in [18]. Specifically, the proposed method can be used to determine a suitable field current in field weakening. The method is a hybrid

Manuscript received 12 July 2023; revised 26 December 2023 and 1 February 2024; accepted 11 March 2024. Date of publication 18 March 2024; date of current version 19 April 2024. This work was supported by the European Commission, through POWERDRIVE project, under Grant 101056857. Recommended for publication by Associate Editor A. M. Trzynadlowski. *(Corresponding author: Junfei Tang.)*

The authors are with the Electric Power Engineering, Chalmers University of Technology, 412 96 Gothenburg, Sweden (e-mail: junfei.tang@chalmers.se; bowen.jiang@chalmers.se; hao.chen@chalmers.se; yujing.liu@chalmers.se; stefan.lundberg@chalmers.se).

Color versions of one or more figures in this article are available at https://doi.org/10.1109/TPEL.2024.3377470.

Digital Object Identifier 10.1109/TPEL.2024.3377470

approach, which is composed of an analytical method, iterative computation, and curve fitting. Nevertheless, this method is complicated since it consists of several iteration loops, and the cost function is limited to total copper losses.

Hence the aim of this study is to find a solution to dynamically determine current references in torque control of EESMs in all working conditions including torque-boosting when one of the stator or rotor current limits is reached and field-weakening when the stator voltage limit is reached. In addition, the cost function to be minimized should be dynamically adjustable. For instance, it can be the total copper losses in normal conditions so that the best efficiency can be achieved, or it can be a weighted function of copper losses in case one of the windings is close to its thermal limit. In the end, the method should be simple to implement without iterative loops so that it can be recognized as a practical solution.

II. Electrical Model of EESM

The electrical characteristics of the machine can be modeled in the *dq*-frame [7], [19]. The Park Transform applied here is amplitude-invariant. The field current is the actual dc current that flows in the field winding without any scaling factor.

A. Electrical Model in Dynamics

The machine electrical dynamics can be described as

$$\boldsymbol{u} = \boldsymbol{R}\boldsymbol{i} + \frac{d\boldsymbol{\psi}}{dt} + \boldsymbol{\omega}\boldsymbol{\psi} \tag{1}$$

where $\boldsymbol{u}$, $\boldsymbol{i}$, and $\boldsymbol{\psi}$ are the vectors of voltages, currents, and flux linkages in *d*-axis, *q*-axis, and field windings, respectively

$$\boldsymbol{u} = \begin{bmatrix} u_{\mathrm{d}} \\ u_{\mathrm{q}} \\ u_{\mathrm{f}} \end{bmatrix}, \quad \boldsymbol{i} = \begin{bmatrix} i_{\mathrm{d}} \\ i_{\mathrm{q}} \\ i_{\mathrm{f}} \end{bmatrix}, \quad \boldsymbol{\psi} = \begin{bmatrix} \psi_{\mathrm{d}} \\ \psi_{\mathrm{q}} \\ \psi_{\mathrm{f}} \end{bmatrix}. \tag{2}$$

$\boldsymbol{R}$ and $\boldsymbol{\omega}$ are the matrices of resistances and speed

$$\boldsymbol{R} = \begin{bmatrix} R_{\mathrm{s}} & 0 & 0 \\ 0 & R_{\mathrm{s}} & 0 \\ 0 & 0 & R_{\mathrm{r}} \end{bmatrix}, \quad \boldsymbol{\omega} = \begin{bmatrix} 0 & -\omega_{\mathrm{r}} & 0 \\ \omega_{\mathrm{r}} & 0 & 0 \\ 0 & 0 & 0 \end{bmatrix}. \tag{3}$$

Here, R_{s} is the resistance of the stator armature winding, R_{f} is the resistance of the rotor field winding, and ω_{r} is the electrical angular speed. The term $\boldsymbol{\omega}\boldsymbol{\psi}$ is the cross-coupling EMF term due to Park Transform.

The derivatives of flux linkages can be further described as the product of incremental inductances and current derivatives

$$\frac{d\boldsymbol{\psi}}{dt} = \boldsymbol{l}\frac{d\boldsymbol{i}}{dt} \tag{4}$$

where $\boldsymbol{l}$ is the matrix of incremental inductances, which is the Jacobian matrix of flux linkages

$$\boldsymbol{l} = \begin{bmatrix} l_{\mathrm{dd}} & l_{\mathrm{dq}} & l_{\mathrm{df}} \\ l_{\mathrm{qd}} & l_{\mathrm{qq}} & l_{\mathrm{qf}} \\ l_{\mathrm{fd}} & l_{\mathrm{fq}} & l_{\mathrm{ff}} \end{bmatrix} = \begin{bmatrix} \frac{\partial \psi_{\mathrm{d}}}{\partial i_{\mathrm{d}}} & \frac{\partial \psi_{\mathrm{d}}}{\partial i_{\mathrm{q}}} & \frac{\partial \psi_{\mathrm{d}}}{\partial i_{\mathrm{f}}} \\ \frac{\partial \psi_{\mathrm{q}}}{\partial i_{\mathrm{d}}} & \frac{\partial \psi_{\mathrm{q}}}{\partial i_{\mathrm{q}}} & \frac{\partial \psi_{\mathrm{q}}}{\partial i_{\mathrm{f}}} \\ \frac{\partial \psi_{\mathrm{f}}}{\partial i_{\mathrm{d}}} & \frac{\partial \psi_{\mathrm{f}}}{\partial i_{\mathrm{q}}} & \frac{\partial \psi_{\mathrm{f}}}{\partial i_{\mathrm{f}}} \end{bmatrix}. \tag{5}$$

In this study, the flux linkages and inductances are described by look-up tables so that iron-core saturation is considered.

With incremental inductances $\boldsymbol{l}$, the current derivatives can be solved, and the dynamic electrical model is established

$$\frac{d\boldsymbol{i}}{dt} = \boldsymbol{l}^{-1}\ \frac{d\boldsymbol{\psi}}{dt} = \boldsymbol{l}^{-1}\ (\boldsymbol{u} - \boldsymbol{R}\boldsymbol{i} - \boldsymbol{\omega}\boldsymbol{\psi}). \tag{6}$$

B. Electrical Model in Steady States

In a steady state, the derivatives of currents in the *dq*-frame are zero so as the derivatives of flux linkages. In this case, (1) becomes

$$\boldsymbol{u} = \boldsymbol{R}\boldsymbol{i} + \boldsymbol{\omega}\boldsymbol{\psi}. \tag{7}$$

Since the flux linkages $\boldsymbol{\psi}$ are also dependent on currents $\boldsymbol{i}$, to know how $\boldsymbol{i}$ can influence $\boldsymbol{u}$ in the end, a matrix of apparent inductances $\boldsymbol{L}$ is introduced so that $\boldsymbol{\psi}$ can be described by $\boldsymbol{i}$

$$\boldsymbol{\psi} = \boldsymbol{L}\boldsymbol{i} \tag{8}$$

where $\boldsymbol{L}$ can be formulated as

$$\boldsymbol{L} = \begin{bmatrix} L_{\mathrm{dd}} & L_{\mathrm{dq}} & L_{\mathrm{df}} \\ L_{\mathrm{qd}} & L_{\mathrm{qq}} & L_{\mathrm{qf}} \\ L_{\mathrm{fd}} & L_{\mathrm{fq}} & L_{\mathrm{ff}} \end{bmatrix} = \begin{bmatrix} \frac{\int l_{\mathrm{dd}} di_{\mathrm{d}}}{i_{\mathrm{d}}} & \frac{\int l_{\mathrm{dq}} di_{\mathrm{q}}}{i_{\mathrm{q}}} & \frac{\int l_{\mathrm{df}} di_{\mathrm{f}}}{i_{\mathrm{f}}} \\ \frac{\int l_{\mathrm{qd}} di_{\mathrm{d}}}{i_{\mathrm{d}}} & \frac{\int l_{\mathrm{qq}} di_{\mathrm{q}}}{i_{\mathrm{q}}} & \frac{\int l_{\mathrm{qf}} di_{\mathrm{f}}}{i_{\mathrm{f}}} \\ \frac{\int l_{\mathrm{fd}} di_{\mathrm{d}}}{i_{\mathrm{d}}} & \frac{\int l_{\mathrm{fq}} di_{\mathrm{q}}}{i_{\mathrm{q}}} & \frac{\int l_{\mathrm{ff}} di_{\mathrm{f}}}{i_{\mathrm{f}}} \end{bmatrix}. \tag{9}$$

Therefore, the steady-state model described in (7) becomes

$$\boldsymbol{u} = \boldsymbol{R}\boldsymbol{i} + \boldsymbol{\omega}\boldsymbol{L}\boldsymbol{i} = (\boldsymbol{R} + \boldsymbol{\omega}\boldsymbol{L})\ \boldsymbol{i}. \tag{10}$$

C. Electromagnetic Torque and Copper Losses

The electromagnetic torque can be formulated as

$$T_{\mathrm{em}} = \frac{3}{2} \cdot p \cdot (\psi_{\mathrm{d}} \cdot i_{\mathrm{q}} - \psi_{\mathrm{q}} \cdot i_{\mathrm{d}}) \tag{11}$$

where p is the number of pole pairs.

The total copper losses are the sum of stator copper losses and rotor copper losses, which can be further reformulated as a combination of three components, the losses in *d*-axis winding $P_{\mathrm{Cu.d}}$, *q*-axis winding $P_{\mathrm{Cu.q}}$ and field winding $P_{\mathrm{Cu.f}}$

$$\begin{aligned} P_{\mathrm{Cu}} &= 3/2 \cdot R_{\mathrm{s}} \cdot \left(i_{\mathrm{d}}^2 + i_{\mathrm{q}}^2\right) + R_{\mathrm{r}} \cdot i_{\mathrm{f}}^2 \\ &= P_{\mathrm{Cu.d}} + P_{\mathrm{Cu.q}} + P_{\mathrm{Cu.f}} \end{aligned} \tag{12}$$

where

$$P_{\mathrm{Cu.d}} = \frac{3}{2} R_{\mathrm{s}} i_{\mathrm{d}}^2, \quad P_{\mathrm{Cu.q}} = \frac{3}{2} R_{\mathrm{s}} i_{\mathrm{q}}^2, \quad P_{\mathrm{Cu.f}} = R_{\mathrm{r}} i_{\mathrm{f}}^2 \tag{13}$$

and the factor 3/2 is from amplitude-invariant Park Transform.

III. Dynamic Current Reference Determination

Due to the third degree of control freedom introduced by the field current, the dynamic current reference determination for EESM is more complicated than that for PMSM. In this section, gradients of torque versus weighted copper losses are introduced to assist the determination. The control diagram is shown in Fig. 1 and the flow chart is shown in Fig. 2. The explanations of each step are given as follows in this section.

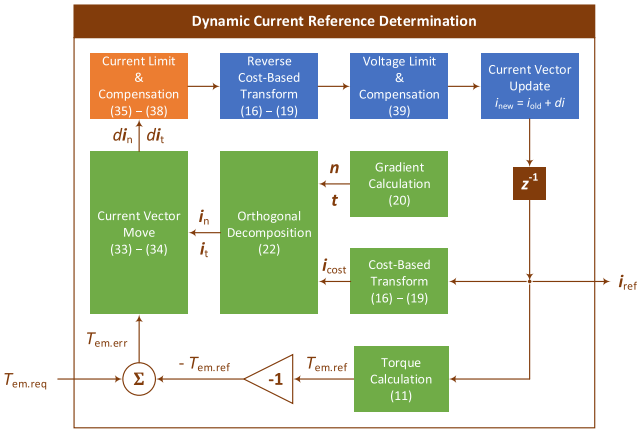

Fig. 1. Schematic diagram of the current reference determination algorithm.

A. Cost Function and Cost-Based Current Frame

The total copper losses P_{Cu} sometimes may not be the target to minimize. For instance, when the rotor winding overheats, the field current should be reduced even if P_{Cu} becomes higher in this case. Therefore, as a general solution, weights can be assigned to the copper losses of each winding individually and a cost function can be defined as

$$P_{\mathrm{cost}} = k_{\mathrm{cost.s}}\, P_{\mathrm{Cu.d}} + k_{\mathrm{cost.s}} P_{\mathrm{Cu.q}} + k_{\mathrm{cost.r}} P_{\mathrm{Cu.f}} \tag{14}$$

where $k_{\mathrm{cost.s}}$ and $k_{\mathrm{cost.f}}$ are the weights for stator and rotor windings respectively. When $k_{\mathrm{cost.s}}$ and $k_{\mathrm{cost.r}}$ are both set to 1, then the cost P_{cost} means the total copper losses P_{Cu}. This is the normal operation mode of the machine when the copper losses should be minimized to achieve the best efficiency. However, if the rotor winding overheats, then $k_{\mathrm{cost.r}}$ can be set higher than $k_{\mathrm{cost.s}}$, so that the algorithm would believe that every watt of rotor copper losses costs more than 1 watt of stator copper losses, and consequently the rotor copper losses will decrease whereas the stator copper losses will increase compared with the normal case. Similarly, $k_{\mathrm{cost.s}}$ can be set higher than $k_{\mathrm{cost.r}}$ when the stator winding overheats.

To simplify the analysis, (14) can be reformulated as

$$P_{\mathrm{cost}} = i_{\mathrm{cost.d}}^2 + i_{\mathrm{cost.q}}^2 + i_{\mathrm{cost.f}}^2 \tag{15}$$

where $i_{\mathrm{cost.d}}$, $i_{\mathrm{cost.q}}$, and $i_{\mathrm{cost.f}}$ can be named cost-equivalent or cost-based currents, which are related to real currents i_{d}, i_{q}, and i_{f}. The relation between can be derived by comparing (13)–(15)

$$i_{\mathrm{cost.d}} = \sqrt{k_{\mathrm{cost.s}} P_{\mathrm{Cu.d}}} = i_{\mathrm{d}}\ \sqrt{3/2 \cdot k_{\mathrm{cost.s}} R_{\mathrm{s}}} = k_{\mathrm{s}}\, i_{\mathrm{d}} \tag{16}$$

$$i_{\mathrm{cost.q}} = \sqrt{k_{\mathrm{cost.s}} P_{\mathrm{Cu.q}}} = i_{\mathrm{q}}\ \sqrt{3/2 \cdot k_{\mathrm{cost.s}} R_{\mathrm{s}}} = k_{\mathrm{s}}\, i_{\mathrm{q}} \tag{17}$$

$$i_{\mathrm{cost.f}} = \sqrt{k_{\mathrm{cost.r}} P_{\mathrm{Cu.f}}} = i_{\mathrm{f}}\ \sqrt{k_{\mathrm{cost.r}} R_{\mathrm{r}}} = k_{\mathrm{r}}\, i_{\mathrm{f}} \tag{18}$$

where k_{s} and k_{r} are the scaling factors between the real currents and the cost-based currents in stator and rotor windings respectively

$$k_{\mathrm{s}} = \sqrt{3/2 \cdot k_{\mathrm{cost.s}} R_{\mathrm{s}}}\,, \qquad k_{\mathrm{f}} = \sqrt{k_{\mathrm{cost.r}} R_{\mathrm{r}}}. \tag{19}$$

In this way, a cost-based frame is established. In this frame, the length of a current vector represents the cost when it is assigned.

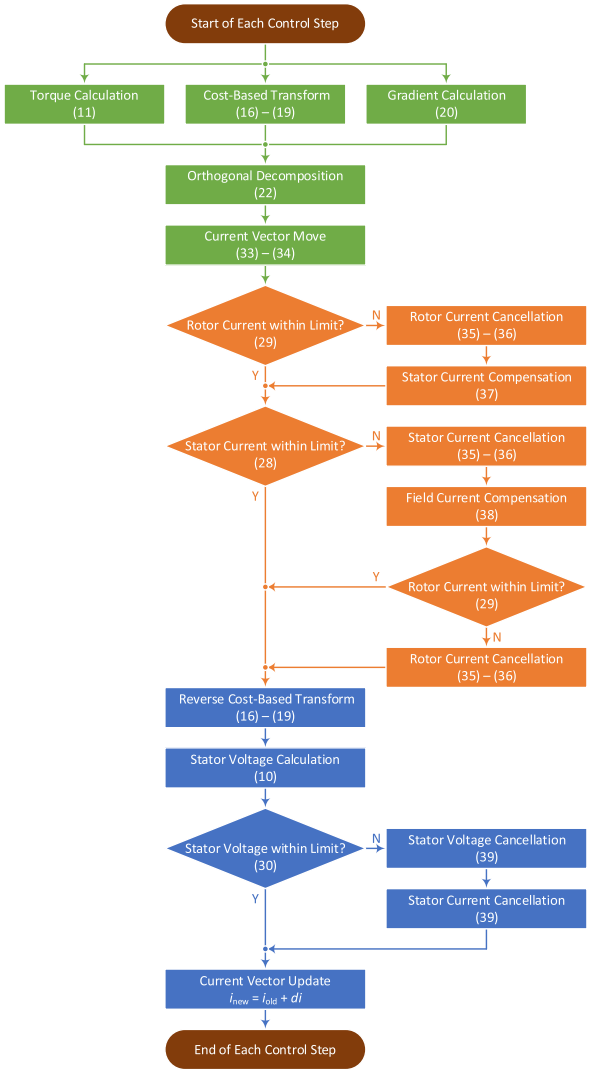

Fig. 2. Flow chart of the current reference determination algorithm.

The determined current vector should therefore be the one that gives the target torque but with minimum length in the cost-based frame.

The weights k_{s} and k_{f} are related to resistances R_{s} and R_{f}. Therefore, a change in temperature, which can be measured using temperature sensors, will cause a change in resistance values, which can be calculated using temperature measurements, and then the ratio between k_{s} and k_{f}. In this way, the weights will be automatically adjusted according to temperature variations, and the electrical load in the stator and rotor will be redistributed correspondingly.

In addition, this cost-based frame can be dynamically adjusted by regulating the weights according to the state of the machine. For instance, when the field winding overheats, $k_{\mathrm{cost.r}}$ can be set higher so that i_{f} is suppressed to reduce copper losses in the field winding. The transform introduced here is shown as the "Cost-Based Transform" block in Figs. 1 and 2.

Since the torque T_{em} is a function of real currents according to (11), T_{em} should also be a function of cost-based currents defined in (16)–(18). Therefore, T_{em} can be described as a scaler

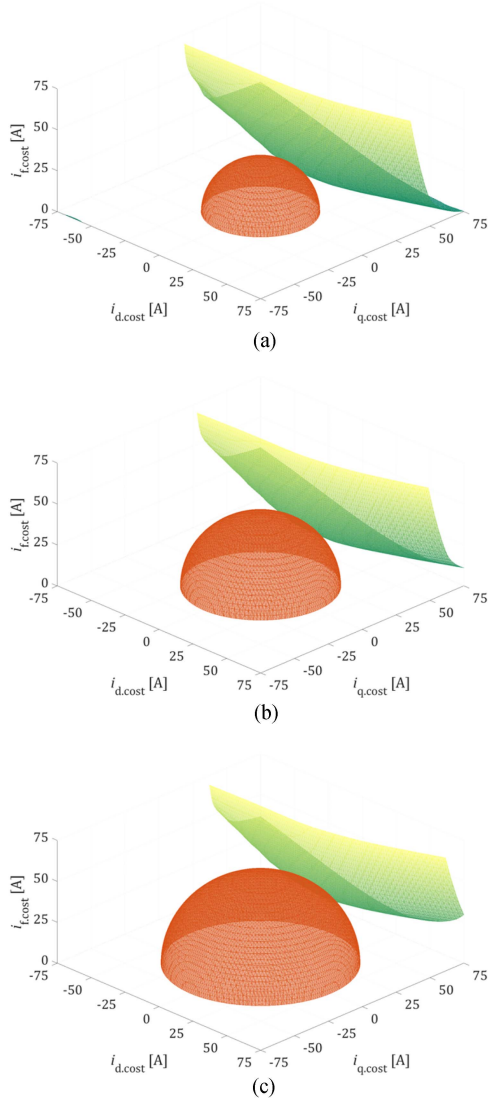

Fig. 3. Iso-surfaces of torque and cost (when $k_{\text{cost.s}} = k_{\text{cost.f}} = 1$, i.e., $P_{\text{cost}} = P_{\text{Cu}}$) with the tangential point in the cost-based current frame at 50, 75, and 100 N·m. The coordinates of the tangential point show the optimum solution of $i_{\text{d.cost}}$, $i_{\text{q.cost}}$, and $i_{\text{f.cost}}$ to reach the specified torque with minimum cost. (a) Iso-surfaces of $T_{\text{em}} = 50$ N·m and $P_{\text{cost}} = 960$ W with tangential point at $i_{\text{d.cost}} = -0.5$ A, $i_{\text{q.cost}} = 26.4$ A, $i_{\text{f.cost}} = 16.2$ A. (b) Iso-surfaces of $T_{\text{em}} = 75$ N·m and $P_{\text{cost}} = 1754$ W with tangential point at $i_{\text{d.cost}} = -3.3$ A, $i_{\text{q.cost}} = 35.7$ A, $i_{\text{f.cost}} = 21.7$ A. (c) Iso-surfaces of $T_{\text{em}} = 100$ N·m and $P_{\text{cost}} = 2699$ W with tangential point at $i_{\text{d.cost}} = -3.6$ A, $i_{\text{q.cost}} = 44.8$ A, $i_{\text{f.cost}} = 26.0$ A.

field in the cost-based current frame. To better illustrate what happens in the cost-based frame, the iso-surfaces of T_{em} and the corresponding iso-surfaces of P_{cost} in tangential are presented in Fig. 3. The iso-surfaces are calculated using the parameters of the EESM prototyped in this study. As can be noticed, when P_{cost} grows from 960 to 1754 W until 2699 W, T_{em} is pushed further away from 50 to 75 N·m until 100 N·m. The tangential points between the T_{em} iso-surfaces and the P_{cost} iso-surfaces show the solutions of $i_{\text{cost.d}}$, $i_{\text{cost.q}}$, and $i_{\text{cost.f}}$ when T_{em} is achieved with the minimum P_{cost}. The tangential points at different T_{em} level will therefore form a trajectory. The current reference determination process is to make sure that the operation point of the machine moves along this trajectory when the torque request

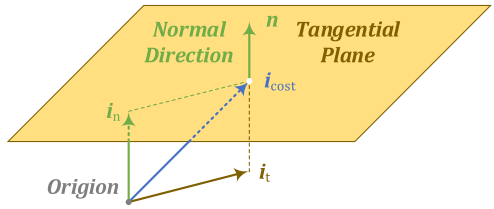

Fig. 4. Orthogonal decomposition of the current vector.

rises or falls. Such trajectory can be obtained by calculating the gradients of T_{em} in the cost-based frame.

B. Gradients of Electromagnetic Torque

From this scaler field, the gradient of torque can be calculated, which establishes a vector field

$$\nabla T_{\text{em.cost}} = \left[\frac{\partial T_{\text{em}}}{\partial i_{\text{cost.d}}} \quad \frac{\partial T_{\text{em}}}{\partial i_{\text{cost.q}}} \quad \frac{\partial T_{\text{em}}}{\partial i_{\text{cost.f}}} \right]^{\text{T}}. \tag{20}$$

This gradient shows the direction in which an increase in torque can be achieved with the minimum cost. Therefore, in case all constraints such as current limits or voltage limits are satisfied, the current vector is supposed to follow a trajectory guided by the direction of this gradient to motivate a torque increase or decrease. This process is shown as the "Gradient Calculation" block in Fig. 2.

C. Orthogonal Decomposition of Current Vector

With the gradient defined in (20), a current vector in the cost-based frame $\boldsymbol{i}_{\text{cost}}$ can be orthogonally decomposed into a normal component $\boldsymbol{i}_{\text{n}}$ that follows this direction and a tangential component $\boldsymbol{i}_{\text{t}}$ that is perpendicular to this direction. Moving $\boldsymbol{i}_{\text{cost}}$ in the direction of $\boldsymbol{i}_{\text{n}}$, the torque increases the fastest, whereas moving the current vector in the direction of $\boldsymbol{i}_{\text{t}}$, the copper losses change whereas the torque remains the same.

Mathematically, this orthogonal decomposition means

$$\boldsymbol{i}_{\text{cost}} = \boldsymbol{i}_{\text{n}} + \boldsymbol{i}_{\text{t}} \quad \& \quad \langle \boldsymbol{i}_{\text{n}}, \boldsymbol{i}_{\text{t}} \rangle = 0. \tag{21}$$

Let $\boldsymbol{n}$ be the unit vector in the normal direction. Then

$$\boldsymbol{i}_{\text{n}} = \langle \boldsymbol{i}_{\text{cost}}, \boldsymbol{n} \rangle \cdot \boldsymbol{n} \quad \& \quad \boldsymbol{i}_{\text{t}} = \boldsymbol{i}_{\text{cost}} - \boldsymbol{i}_{\text{n}}. \tag{22}$$

Let $\boldsymbol{t}$ be the unit vector in the tangential direction, i.e., the direction of $\boldsymbol{i}_{\text{t}}$. Then the inner product of $\boldsymbol{n}$ and $\boldsymbol{t}$ gives zero

$$\langle \boldsymbol{n}, \boldsymbol{t} \rangle = 0. \tag{23}$$

The length of the tangential component $\|\boldsymbol{i}_{\text{t}}\|$ represents the amount of cost that can be possibly reduced. When the minimum cost is achieved, $\boldsymbol{i}_{\text{cost}}$ is perpendicular to the torque contour, which means $\boldsymbol{i}_{\text{cost}} = \boldsymbol{i}_{\text{n}}$ and $\boldsymbol{i}_{\text{t}} = 0$. Hence to reduce the cost means to reduce $\|\boldsymbol{i}_{\text{t}}\|$ as much as possible. This process is illustrated in Fig. 4 and it is shown as the "Orthogonal Decomposition" block in Figs. 1 and 2.

D. Constraints (Voltage Limits and Current Limits)

The determined current references should follow the constraints of current and voltage limits. The armature currents in

the stator should follow

$$i_{\mathrm{d}}^2 + i_{\mathrm{q}}^2 \leq I_{\mathrm{s.max}}^2 \tag{24}$$

where $I_{\mathrm{s.max}}$ is the maximum amplitude of the stator armature current, while the field current in the rotor should follow

$$I_{\mathrm{f.min}} \leq i_{\mathrm{f}} \leq I_{\mathrm{f.max}} \tag{25}$$

where $I_{\mathrm{f.max}}$ is the maximum rotor field current and $I_{\mathrm{f.min}}$ is the minimum rotor field current, which is zero in this study. These constraints can be transformed into the cost-based current frame introduced in the previous section

$$I_{\mathrm{cost.s.max}} = k_{\mathrm{s}}\, I_{\mathrm{s.max}} \tag{26}$$

$$I_{\mathrm{cost.f.max}} = k_{\mathrm{r}}\, I_{\mathrm{f.max}} \ , \ \ I_{\mathrm{cost.f.min}} = k_{\mathrm{r}}\, I_{\mathrm{f.min}}. \tag{27}$$

Therefore, (24) and (25) can be reformulated as

$$i_{\mathrm{cost.d}}^2 + i_{\mathrm{cost.q}}^2 \leq I_{\mathrm{cost.s.max}}^2 \tag{28}$$

$$I_{\mathrm{cost.f.min}} \leq i_{\mathrm{cost.f}} \leq I_{\mathrm{cost.f.max}}. \tag{29}$$

The stator voltage should follow

$$u_{\mathrm{d}}^2 + u_{\mathrm{q}}^2 \leq U_{\mathrm{s.max}}^2 \tag{30}$$

where $U_{\mathrm{s.max}}$ is the maximum amplitude of the stator armature voltage.

In field excitation, to motivate a desirable di_{f}/dt in dynamic control, the field voltage during transient should be higher than that in steady state

$$U_{\mathrm{f.min}} \leq R_{\mathrm{f}} I_{\mathrm{f.min}} \leq R_{\mathrm{f}} i_{\mathrm{f.ref}} \leq R_{\mathrm{f}} I_{\mathrm{f.max}} \leq U_{\mathrm{f.max}} \tag{31}$$

where $U_{\mathrm{f.max}}$ and $U_{\mathrm{f.min}}$ are the maximum and minimum voltage outputs from the field excitation converter. Besides, since there is no speed-dependent EMF term in the field excitation circuit, (31) is valid for the entire speed range. This means that the field voltage corresponding to any field current reference will never exceed the voltage limit of the field excitation converter. Therefore, the voltage constraints for the field winding do not need to be considered in the current reference determination process.

E. Move of Current Vector Without Constraints

When a torque request $T_{\mathrm{em.req}}$ is sent to the current reference determination algorithm, the algorithm starts to move the current vector to achieve the torque request while minimizing the cost. Similarly, the move, $d\boldsymbol{i}_{\mathrm{cost}}$, can be orthogonally decomposed into components along normal and tangential directions

$$d\boldsymbol{i}_{\mathrm{cost}} = d\boldsymbol{i}_{\mathrm{n}} + d\boldsymbol{i}_{\mathrm{t}} \quad \& \quad \langle d\boldsymbol{i}_{\mathrm{n}},\, d\boldsymbol{i}_{\mathrm{t}} \rangle = 0 \tag{32}$$

where $d\boldsymbol{i}_{\mathrm{n}}$ is the move to penetrate the torque contour in the normal direction $\boldsymbol{n}$, whereas $d\boldsymbol{i}_{\mathrm{t}}$ is the move to slide along the torque contour in the tangential direction $\boldsymbol{t}$.

As for $d\boldsymbol{i}_{\mathrm{n}}$, the length should be proportional to the difference between the torque request $T_{\mathrm{em.req}}$ and the amount of torque that is already achieved by the current references $T_{\mathrm{em.ref}}$. In addition, the length of $d\boldsymbol{i}_{\mathrm{n}}$ should be reversely proportional to the amount of torque increase due to the per unit increase of $\boldsymbol{i}_{\mathrm{n}}$, which is actually the length of $\nabla T_{\mathrm{em.cost}}$. Hence

$$d\boldsymbol{i}_{\mathrm{n}} = k_{\mathrm{n}} \cdot \frac{T_{\mathrm{em.req}} - T_{\mathrm{em.ref}}}{\|\nabla T_{\mathrm{em.cost}}\|} \cdot T_{\mathrm{ctrl}} \cdot \boldsymbol{n} \tag{33}$$

where k_{n} is the bandwidth in Hz and T_{ctrl} is the control time step.

As for $d\boldsymbol{i}_{\mathrm{t}}$, the current reference vector needs to move in the reverse direction of $\boldsymbol{i}_t$ to reduce $\|\boldsymbol{i}_{\mathrm{t}}\|$. Hence

$$d\boldsymbol{i}_{\mathrm{t}} = -k_{\mathrm{t}} \cdot T_{\mathrm{ctrl}} \cdot \boldsymbol{i}_{\mathrm{t}} \tag{34}$$

where k_{t} is the bandwidth in Hz.

A higher k_{n} means a faster achievement of torque, whereas a higher k_{t} means a faster minimization of cost. This process is shown as the "Current Vector Move" block in Figs. 1 and 2.

F. Current Reference Determination With Current Limits

When a move of the current vector tends to break any current limit, a cancellation vector $d\boldsymbol{i}_{\mathrm{cancel.i}}$ needs to be generated to restrain the current vector within the limit

$$d\boldsymbol{i}_{\mathrm{lim}} = d\boldsymbol{i}_{\mathrm{cost}} - d\boldsymbol{i}_{\mathrm{cancel.i}} \tag{35}$$

where $d\boldsymbol{i}_{\mathrm{lim}}$ is the limited move of the current vector and

$$d\boldsymbol{i}_{\mathrm{cancel.i}} = \begin{bmatrix} i_{\mathrm{cancel.d}} & i_{\mathrm{cancel.q}} & i_{\mathrm{cancel.f}} \end{bmatrix}^{\mathrm{T}}. \tag{36}$$

Such cancellation mechanism under the current limitation is illustrated in Fig. 5.

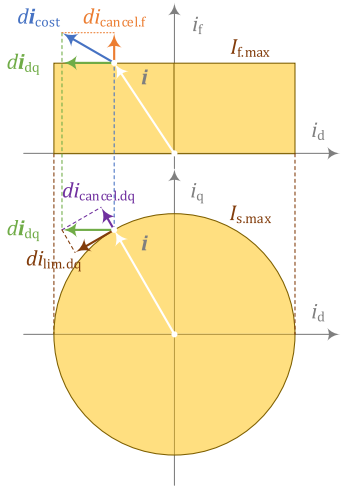

Fig. 5. Current reference determination with current limits.

Introducing such a cancellation will lead to a loss of torque and furthermore, a delay in response of torque reference. Therefore, if possible, the loss due to the limitation of one current should be compensated by an increase of other currents. For instance, when the field current limit is reached, the loss of torque due to $i_{\mathrm{cancel.f}}$, which is $i_{\mathrm{cancel.f}} \frac{\partial T_{\mathrm{em}}}{\partial i_{\mathrm{cost.f}}}$, should be compensated by an increase of $i_{\mathrm{cost.d}}$ and $i_{\mathrm{cost.q}}$. This compensation should be in the direction of the gradient on the dq-plane so that every ampere is spent the most effectively and with a proper length so that the compensation is exact. Practically, the compensation can be formulated as a cancellation with a negative sign so that (35) is

TABLE I
EESM PARAMETERS

Parameter		Value	Unit
lamination stack length		120.0	mm
stator outer diameter		175.0	mm
stator inner diameter		123.0	mm
rotor outer diameter		121.6	mm
number of turns in stator winding	per pole	4	
number of turns in rotor winding	per pole	112	
Stator Lamination Material		B35AV1900	
Rotor Lamination Material		M235-35A	
Shaft Material		C45E (SS1672)	

universal

$$\begin{bmatrix} di_{\text{cancel.d}} \\ di_{\text{cancel.q}} \end{bmatrix} = -\frac{i_{\text{cancel.f}} \frac{\partial T_{\text{em}}}{\partial i_{\text{cost.f}}}}{\left(\frac{\partial T_{\text{em}}}{\partial i_{\text{cost.d}}}\right)^2 + \left(\frac{\partial T_{\text{em}}}{\partial i_{\text{cost.q}}}\right)^2} \begin{bmatrix} \frac{\partial T_{\text{em}}}{\partial i_{\text{cost.d}}} \\ \frac{\partial T_{\text{em}}}{\partial i_{\text{cost.q}}} \end{bmatrix}. \quad (37)$$

The compensation for the loss of torque due to $i_{\text{cancel.d}}$ and $i_{\text{cancel.q}}$ is simpler

$$d\, i_{\text{cancel.f}} = -\frac{i_{\text{cancel.d}} \frac{\partial T_{\text{em}}}{\partial i_{\text{cost.d}}} + i_{\text{cancel.q}} \frac{\partial T_{\text{em}}}{\partial i_{\text{cost.q}}}}{\frac{\partial T_{\text{em}}}{\partial i_{\text{cost.f}}}}. \quad (38)$$

After the compensation, the limits are to be checked again to make sure that they are not exceeded due to compensation. This entire process is shown as the orange blocks in Figs. 1 and 2.

G. Current Reference Determination With Voltage Limits

The voltage limits are checked in the real current frame. First, the current vector is transformed from the cost-based current frame to the real current frame. Then the stator voltage is calculated according to (7). In case of a move of current vector tending to break the voltage limit, a cancellation vector $d\boldsymbol{u}_{\text{cancel.u}}$ is generated to restrain the voltage vector within the limit. Then $d\boldsymbol{u}_{\text{cancel.u}}$ will be transformed into a cancellation vector of currents $d\boldsymbol{i}_{\text{cancel.u}}$

$$d\boldsymbol{i}_{\text{cancel.u}} = (\boldsymbol{R} + \boldsymbol{\omega L})^{-1}\, d\boldsymbol{u}_{\text{cancel.u}}. \quad (39)$$

Similarly, this cancellation will lead to a loss of torque. To compensate for this, $d\boldsymbol{i}_{\text{cancel.u}}$ is again transformed into the cost-based frame and then the compensation method is the same as described in (37) and (38). This process is shown as the blue blocks in Figs. 1 and 2.

IV. Performance Evaluation

To evaluate the proposed control algorithm, an EESM is prototyped. The EESM stator has three phases, eight poles, and 48 slots. The stator windings are made of hairpins while the rotor winding is made of strands of 1 mm diameter. The parameters of the machine are shown in Table I. Two PT100 RTD sensors are installed in the stator windings while one Type K thermocouple is installed in the rotor winding. The temperature measurements are used to update the resistance values in the controller and further the weights k_{s} and k_{f} according to (19). The field excitation of EESM is brushless. A two-channel telemetry is implemented to feedback on the measurements of field current and rotor winding temperature to the controller.

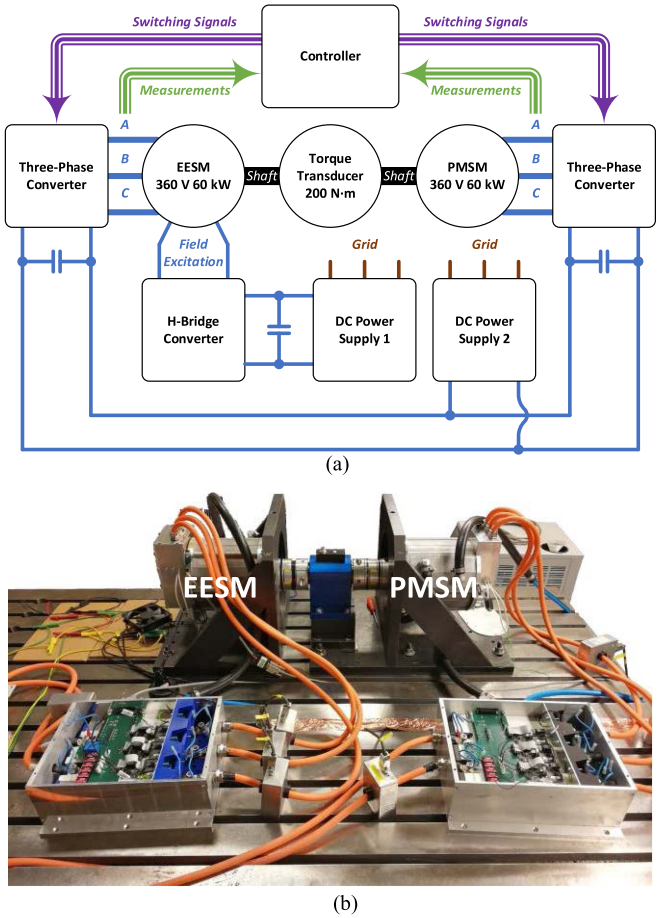

(a)

(b)

Fig. 6. Test setup with EESM and PMSM back-to-back connected. (a) Schematic diagram of the test setup. (b) Photograph of the test setup.

The EESM is connected back-to-back to a PMSM on a test bench. The schematic diagram of the setup is shown in Fig. 6(a) and a photograph of the test bench is shown in Fig. 6(b). In the test, the PMSM is in speed control whereas the EESM is in torque control. The control is implemented in SCALEXIO. The control signals are updated per switching cycle at 10 kHz.

The evaluation process of this study is to verify whether current references in EESM control can be dynamically determined using the proposed method, which is based on torque gradients and orthogonal decomposition instead of using precalculated look-up tables. In the evaluation process, k_{n} is selected as 10, whereas k_{t} is selected as 1. The selection is made through trial and error to have the response fast enough while overshot is avoided. $k_{\text{cost.r}}$ is switched between 0.5, 1, and 2 so that the change of current distributions between stator and rotor windings can be observed. Obviously, increasing $k_{\text{cost.r}}$ is equivalent to decreasing $k_{\text{cost.s}}$ and vice versa. All results presented in this section are experimental. Typical cases are studied to evaluate the method with or without the voltage or current limits reached. Results are presented as follows.

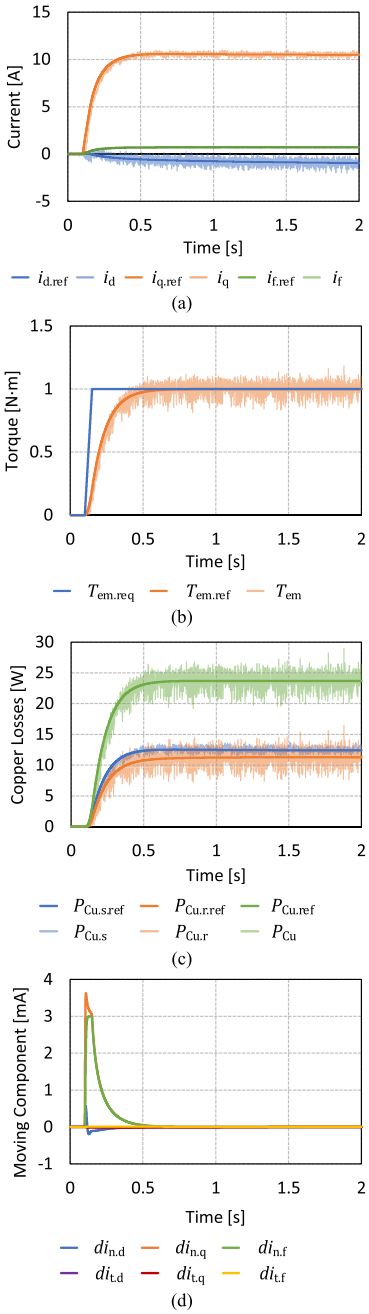

Fig. 7. Responses of current references, currents, torque references, torque, copper losses, normal moving vector, and tangential moving vector when a step of the torque request $T_{em.req}$ from 0 to 1 N·m is applied at 0.1 s whereas the weight of field copper losses $k_{cost.r}$ is fixed at 1 N·m.

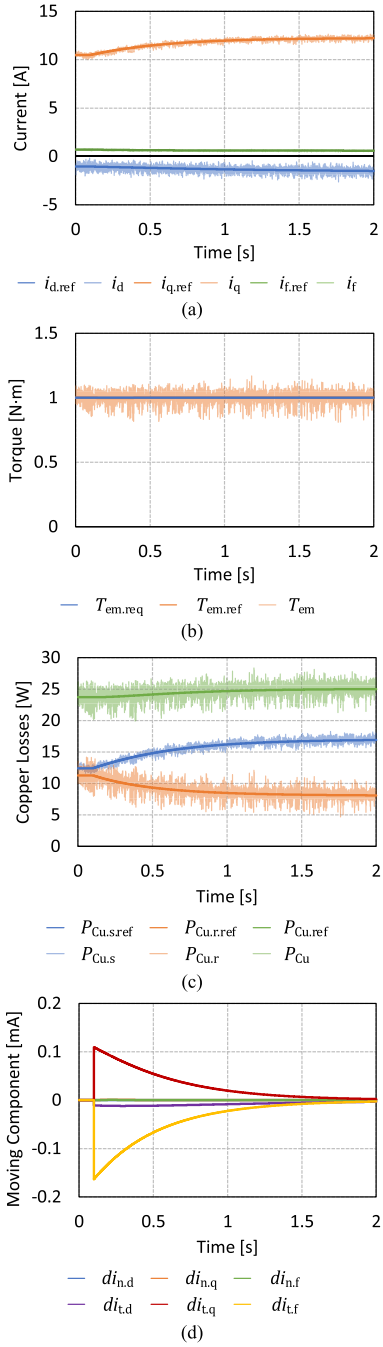

Fig. 8. Responses of current references, currents, torque references, torque, copper losses, normal moving vector, and tangential moving vector when a step of the weight of field copper losses $k_{cost.r}$ from 1 to 2 is applied at 0.1 s whereas the torque request $T_{em.req}$ is fixed at 1 N·m.

A. *Determination Within Current and Voltage Limits*

In this scenario, the EESM rotates at 400 r/min. The first test is a step response of a torque request. In this case, a step of $T_{em.req}$ from 0 to 1 N·m is applied at 0.1 s while $k_{cost.r}$ is fixed at 1.

The responses are shown in Fig. 7. As can be noticed, the normal vector responds immediately after the torque request is set as shown in Fig. 7(d). This motivates the current reference vector as shown in Fig. 7(a) and as a result, the torque catches the request within 0.5 s as shown in Fig. 7(b). In contrast to the active normal vector, the tangential vector is silent during this transient. This is as expected because the current vector follows the trajectory of the torque gradient to form a torque rise. Hence there is no need to adjust the vector to reduce the cost since the cost is already minimized along the trajectory. This clearly shows that the normal vector is purely related to torque increase without generating any unnecessary cost. In addition, the copper losses of the stator and rotor rise simultaneously as shown in Fig. 7(c). It is shown later in comparison that this solution gives the minimum copper losses.

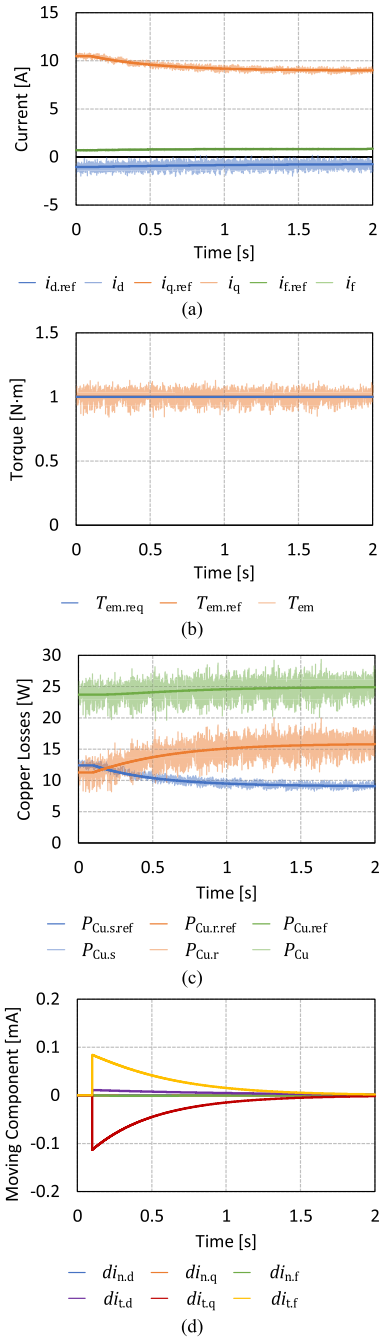

Fig. 9. Responses of current references, currents, torque references, torque, copper losses, normal moving vector, and tangential moving vector when a step of the weight of field copper losses $k_{\text{cost.r}}$ from 1 to 0.5 is applied at 0.1 s whereas the torque request $T_{\text{em.req}}$ is fixed at 1 N·m.

Then the step response of change of weights in cost function is tested. In this case, $k_{\text{cost.r}}$ is switched from 1 to 2 at 0.1 s whereas $T_{\text{em.req}}$ is fixed at 1 N·m. The results are shown in Fig. 8. Due to the increase of the weight assigned to rotor copper losses in the cost function, the controller tends to use more stator current instead of rotor current. Consequently, the tangential vector responds immediately as shown in Fig. 8(d) and then the currents start to adjust accordingly as shown in Fig. 8(a). In contrast to the active tangential vector, the normal vector is silent in this case. As a result, the torque remains the same as shown in Fig. 8(b) whereas the copper losses of the stator and rotor start to deviate as shown in Fig. 8(c) and the total copper losses increase. This clearly shows that the tangential vector is only related to cost reduction while not affecting the torque. The opposite situation is shown in Fig. 9 where $k_{\text{cost.r}}$ is switched from 1 to 0.5 at 0.1 s whereas $T_{\text{em.req}}$ is fixed at 1 N·m.

Comparing Figs. 7–9(c), any deviation from the solution presented in Fig. 7(c) will lead to a higher amount of total copper losses. This means that the minimum amount of total copper losses is achieved in Fig. 7(c) where the total copper losses are actually set as the cost function. In addition, relating Figs. 7–9(b)–(d), it can be concluded that the normal vector is purely related to torque increase without making any unnecessary cost whereas the tangential vector is purely related to cost reduction without affecting the torque.

In summary, the orthogonal decomposition and cost minimization proposed in this study work successfully. Until now, the functions of the green blocks in Fig. 2 are verified.

B. Determination With Current Limits Reached

In this case, a higher torque is requested so that the current limit can be reached. The stator current limit is set at 15 A whereas the rotor current limit is set at 3 A. It should be pointed out that the current limits set here are not the physical limits. Instead, they are the ones intentionally set lower than the physical ones so that the response of the control algorithm when the limits are reached can be evaluated.

The responses are shown in Fig. 10. A torque step from 1 to 2 N·m is applied at 0.1 s as can be seen in Fig. 10(b). The normal vector responses immediately as shown in Fig. 10(d). As a result, the currents response correspondingly as shown in Fig. 10(a), and the torque follows the request as shown in Fig. 10(b). The stator current limit is hit at 0.3462 s. Thereafter, the current limit cancellation vector is activated to constrain the current vector inside the boundary as can be seen in Fig. 10(f). From here on, due to the impact of the cancellation vector, the current vector starts to deviate from the original trajectory of minimum copper losses. This is why the tangential vector responses fiercely trying to bring the vector back to the original trajectory as shown in Fig. 10(e). Thereafter, as time approaches, the cancellation vector and tangential vector gradually come into balance, and they eventually meet each other at around 0.9 s.

To evaluate the capability to dynamically redistribute the load between stator and rotor windings when current limits are reached, at 1 s, $k_{\text{cost.r}}$ is stepped from 1 to 0.5. This encourages the controller to increase the usage of field current rather than stator current. Therefore, as can be noticed, the same as in the previous case, the tangential vector responses immediately as shown in Fig. 10(e), whereas the normal vector remains the same as shown in Fig. 10(d). Consequently, the stator current decreases whereas the field current increases as shown in Fig. 10(a). At the same time, since the tangential vector brings the stator current lower, the current vector detaches the limit, and therefore, the cancellation vector drops to zero as can be seen in Fig. 10(f). In addition, the responses of stator and rotor currents

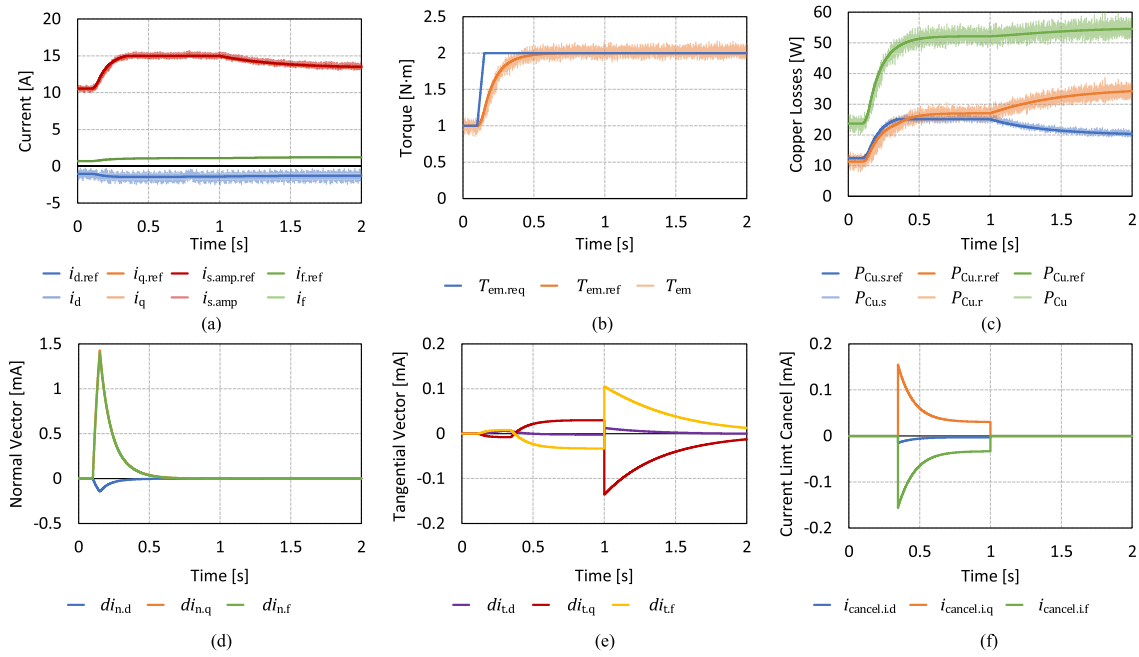

Fig. 10. Responses of current references, currents, torque references, torque, copper losses, normal moving vector, and tangential moving vector when a step of torque request $T_{\mathrm{em.req}}$ from 0 to 1 N·m is applied and when the weight of field copper losses $k_{\mathrm{cost.r}}$ is adjusted between 1 and 0.5. (a) Current references and currents. (b) Request, reference, and actual value of torque. (c) Copper losses. (d) Normal vector in the cost-based frame. (e) Tangential vector in the cost-based frame. (f) Current limit cancellation vector.

lead to an increase in rotor copper losses and a decrease in stator copper losses. As a result, the total copper losses increase as shown in Fig. 10(c). This shows that the determination of current references to minimize the cost function still works as expected even when the current limit is reached.

In summary, the cancellation mechanism proposed in this study to restrain the current vector from exceeding the limit works successfully. In this section, the functions of the orange blocks in Fig. 2 are verified.

C. Determination With Voltage and Current Limits Reached

This is the most extreme scenario in which both voltage and current limits are reached simultaneously. In this case, to reach the stator voltage limit, the speed of the machine increases from 600 to 650 r/min whereas the torque request is fixed at 2.5 N·m. The stator voltage limit is set at 9 V. Again, this is not the physical voltage limit. Instead, this value is set intentionally lower than the physical one so that the function of the algorithm when the voltage limit is reached can be evaluated.

The responses are shown in Fig. 11. In the beginning, the stator current is already saturated as can be seen in Fig. 11(a). The current limit cancellation vector and the tangential vector keep in balance as shown in Fig. 11(f) and (h), which has been explained in the previous case. At this moment, the stator voltage is also very close to the limit as shown in Fig. 11(d). Then the speed starts to increase at 0.5 s as shown in Fig. 11(g) and the voltage saturates soon after that. The voltage limit cancellation vector responses immediately as shown in Fig. 11(i). This yields a higher negative d-axis current as shown in Fig. 11(a). This is as expected since a negative d-axis current will generate a negative d-axis flux, which will cancel part of the rotor field excitation and reduce the back-EMF in the stator winding. However, introducing additional negative d-axis current leads to a reduction of positive q-axis current since the stator current limit is already reached, and this means that the current vector deviates from the trajectory of torque gradient even further. Consequently, the torque decreases as shown in Fig. 11(b). The discrepancy between the torque request and the torque generated furthermore activates the normal vector as shown in Fig. 11(e). Moreover, the deviation of the current vector from the trajectory of the torque gradient also means an increase in the cost since the minimum cost is always along the trajectory. Hence the tangential vector also reacts trying to bring the vector back to the optimum trajectory as shown in Fig. 11(f). The transients end when the speed reaches 650 r/min. Thereafter, the normal vector, tangential vector, current limit cancellation vector, and voltage limit cancellation vector keep in balance and the current vector starts to stabilize.

In addition, as can be noticed from Fig. 11(h) and (i), for the duration when both current and voltage cancellation vectors are activated, the cancellation vectors are in the shape of pulses. This is because when the voltage cancellation is activated, the current vector is moved in the direction where the voltage can be reduced the most effectively. However, movement in such direction also detaches the current vector from the current limit. Consequently, the current limit cancellation is deactivated. Thereafter, the normal vector motivates the current vector to increase again trying to meet the torque request. This continues until the current limit is hit again. When the current limit is reached, the current cancellation activates, and the current vector is directed to shrink the most effectively. However, moving in

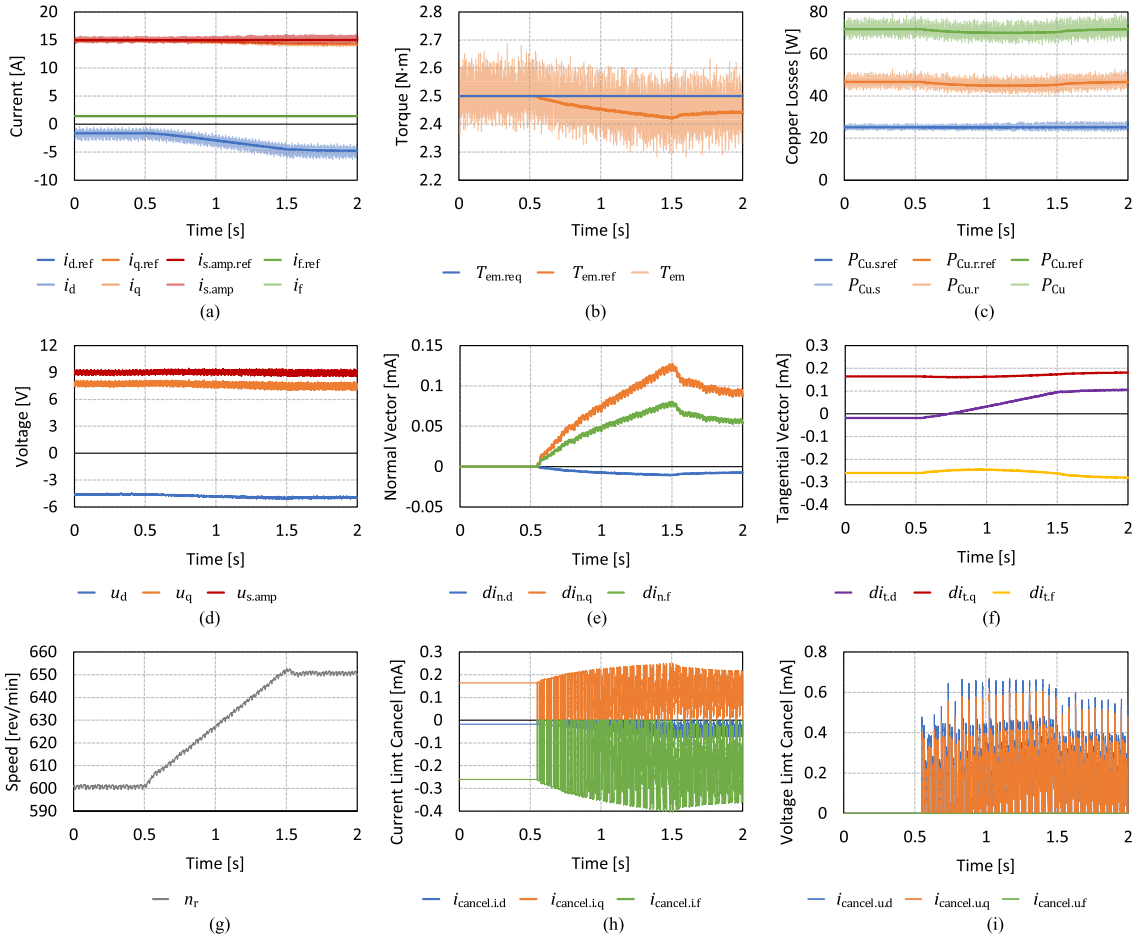

Fig. 11. Responses of current references, currents, torque references, torque, copper losses, normal moving vector, tangential moving vector, and cancellation vectors when the machine accelerates from 600 to 650 r/min during 0.5–1.5 s. The weight of field copper losses $k_{cost.r}$ is fixed at 1. (a) Current references and currents. (b) Request, reference, and actual value of torque. (c) Copper losses. (d) Stator voltages. (e) Normal vector. (f) Tangential vector. (g) Speed. (h) Current limit cancellation. (i) Voltage limit cancellation.

such direction, the voltage limit is detached. Consequently, the voltage cancellation deactivates. This is how the voltage and current cancellation vectors take turns to activate and deactivate in such a scenario. It should be emphasized that this shape of pulses does not indicate any failure of the algorithm. In fact, all components behave as expected in this scenario.

In summary, the cancellation mechanism proposed in this study to restrain the voltage vector from exceeding the limit works successfully. In this section, the functions of the blue blocks in Fig. 2 are verified. Until now, all blocks in the entire flow chart have been evaluated.

V. Conclusion

An algorithm is proposed in this article to dynamically determine the current references in EESM torque control. There are two major contributions from this research.

1) The stator current and rotor current can be dynamically redistributed to minimize the total copper losses during temperature variations while maintaining the same torque. This is achieved by adopting an adaptive cost function proposed in this study. In this function, the cost is defined as the sum of stator and rotor copper losses with separate weights.
2) The torque and copper losses can be controlled separately. This is achieved by adopting an orthogonal decomposition method proposed in this study. In this method, following the direction of torque gradients versus copper losses, the torque increases with the minimum cost, whereas following an orthogonal direction, the cost reduces without any change of torque. The current vector, therefore, moves in a combination of these two directions to achieve the target torque while minimizing the cost.

The algorithm is evaluated in experiments. It is shown that, with the orthogonal decomposition method applied, the control of torque and the control of copper losses are effectively decoupled. The target torque is achieved while the cost is minimized successfully. When the weights for the stator and copper losses change, the distribution of load on stator and rotor currents adjusts automatically. Adopting a vector cancellation technique proposed in this study, the algorithm still works as expected when the current limits or voltage limits are reached. The algorithm works even in the most extreme case when both voltage and current limits are reached simultaneously.

ACKNOWLEDGMENT

The opinions expressed in this document reflect only the authors' view and reflect in no way the European Commission's opinions. The European Commission is not responsible for any use that may be made of the information it contains.

REFERENCES

[1] International Energy Agency, "Global EV outlook 2023," International Energy Agency, 2023. [Online]. Available: https://www.iea.org/reports/global-ev-outlook-2023

[2] E. M. Illiano, "Design of a highly efficient brushless current excited synchronouos motor for automotive purposes," Ph.D. dissertation, Swiss Federal Inst. Technol. Zurich (ETH Zurich), Zurich, Switzerland, 2014.

[3] Renault Group, "The renault ZOE motor: Energy efficiency and power!," Renault Group, Mar. 8, 2021. Accessed: Jul. 4, 2023. [Online]. Available: https://www.renaultgroup.com/en/news-on-air/news/the-renault-zoe-motor-energy-efficiency-and-power/

[4] BRUSA Elektronik AG, "Design of a brushless separately excited synchronous motor," Accessed: Jul. 4, 2023. [Online]. Available: https://ethz.ch/content/dam/ethz/special-interest/mavt/energy-science-center-dam/events/frontiers-presentations/140218_FiER_Illiano.pdf

[5] MAHLE GmbH, "MAHLE develops highly efficient magnet-free electric motor," MAHLE GmbH, May 5, 2021. Accessed: Jul. 4, 2023. [Online]. Available: https://newsroom.mahle.com/press/en/press-releases/mahle-develops-highly-efficient-magnet-free-electric-motor--82368

[6] BMW Group, "The BMW i7 M70 xDrive," BMW Group, Apr. 17, 2023. Accessed: Jul. 4, 2023. [Online]. Available: https://www.press.bmwgroup.com/global/article/detail/T0412894EN/the-bmw-i7-m70-xdrive

[7] J. Tang and Y. Liu, "Design of electrically excited synchronous machines to achieve unity power factor in field weakening for long-haul electric trucks," in *Proc. Int. Conf. Elect. Machines*, 2020, pp. 422–428.

[8] C. Stancu, T. Ward, K. M. Rahman, R. Dawsey, and P. Savagian, "Separately excited synchronous motor with rotary transformer for hybrid vehicle application," *IEEE Trans. Ind. Appl.*, vol. 54, no. 1, pp. 223–232, Jan./Feb. 2018.

[9] A. D. Gioia et al., "Design and demonstration of a wound field synchronous machine for electric vehicle traction with brushless capacitive field excitation," *IEEE Trans. Ind. Appl.*, vol. 54, no. 2, pp. 1390–1403, Mar./Apr. 2018.

[10] J. Choi, I. Jeong, K. Nam, and S. Jung, "Sensorless control for electrically energized synchronous motor based on signal injection to field winding," in *Proc. IECON-39th Annu. Conf. IEEE Ind. Electron. Soc.*, 2013, pp. 3120–3129.

[11] J. Kou, Q. Gao, K. Xu, and D. Xu, "A sensorless rotor position estimation method based on the field current harmonic for an LCI-Fed EESM," *IEEE Trans. Ind. Electron.*, vol. 66, no. 4, pp. 2561–2569, Apr. 2019.

[12] Y. Zhou and S. Long, "Sensorless direct torque control for electrically excited synchronous motor based on injecting high-frequency ripple current into rotor winding," *IEEE Trans. Energy Convers.*, vol. 30, no. 1, pp. 246–253, Mar. 2015.

[13] O. Haala, B. Wagner, M. Hofmann, and M. März, "Optimal current control of externally excited synchronous machines in automotive traction drive applications," *Int. J. Elect., Comput., Energetic, Electron. Commun. Eng.*, vol. 7, no. 9, pp. 1133–1139, 2013.

[14] R. Wang, S. Pekarek, and M. Bash, "Alternative excitation strategies for a wound rotor synchronous machine drive," in *Proc. IEEE Energy Convers. Congr. Expo.*, 2012, pp. 2300–2307.

[15] K. Liang, W. Xuhui, and F. Tao, "A new method to plan the optimal field excitation current trajectory in a hybrid excitation machine," in *Proc. Int. Conf. Elect. Mach. Syst.*, 2011, pp. 1–5.

[16] J. Tang and Y. Liu, "Comparison of copper loss minimization and field current minimization for electrically excited synchronous motor in mild hybrid drives," in *Proc. 19th Eur. Conf. Power Electron. Appl.*, 2017, pp. P.1–P.10.

[17] J. Tang, "Machine performance in steady state," in *Design and Control of Electrically Excited Synchronous Machines for Vehicle Applications*. Gothenburg, Sweden: Chalmers Univ. Technol., 2021, pp. 27–53.

[18] Y. Kim and K. Nam, "Copper-loss-minimizing field current control scheme for wound synchronous machines," *IEEE Trans. Power Electron.*, vol. 32, no. 2, pp. 1335–1345, Feb. 2017.

[19] J. Tang, "Machine modeling," in *Design and Control of Electrically Excited Synchronous Machines for Vehicle Applications*. Gothenburg, Sweden: Chalmers Univ. Technol., 2021, pp. 11–25.

Junfei Tang (Member, IEEE) received the B.Eng. degree in electrical engineering from Jiangsu University, Zhenjiang, China, in 2013, and the M.Sc. and Ph.D. degrees in electric power engineering from Chalmers University of Technology, Gothenburg, Sweden, in 2016 and 2021, respectively.

He is currently a Postdoctoral Researcher with Chalmers University of Technology. His research interests include design and control of electric machines and power electronics.

Dr. Tang was acknowledged as a star reviewer for 2020 by the IEEE Power & Energy Society.

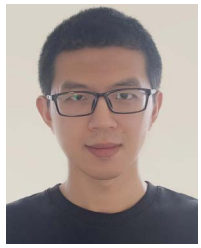

Bowen Jiang (Graduate Student Member, IEEE) received the M.Sc. degree in automotive engineering, in 2020, from Chalmers University of Technology, Gothenburg, Sweden, where he is currently working toward the Ph.D. degree in electrical engineering. His current research interests include parameter identification and dynamic control of electric machines.

Hao Chen (Member, IEEE) received the B.Sc. degree in electrical engineering from the School of Electrical Engineering, Beijing Jiaotong University, Beijing, China, in 2012, and the Ph.D. degree in control science and engineering from the School of Automation, Beijing Institute of Technology, Beijing, China, in 2019.

From 2016 to 2018, he was with the Department of Electrical and Computer Engineering, Marquette University, Milwaukee, WI, USA, as a Joint Ph.D. Student. From 2019 to 2021, he was a Postdoctoral Research Fellow with Nanyang Technological University, Singapore. He is currently a Researcher with the Department of Electrical Engineering, Chalmers University of Technology, Gothenburg, Sweden. His research interests include the design and optimization of electric machines, power electronic drives, and motor control.

Yujing Liu (Senior Member, IEEE) received the B.Sc., M.Sc., and Ph.D. degrees in electrical engineering from Harbin Institute of Technology, Harbin, China, in 1982, 1985, and 1988, respectively.

In 1996–2013, he worked in ABB Corporate Research, Västerås, Sweden. Since 2013, he has been a Professor of electrical power engineering with Chalmers University of Technology, Gothenburg, Sweden. His research interests include the research on motors, converters, and wireless charging for electric vehicles, generators and power electronics for tidal power conversion, and high efficiency machines for energy saving in industrial applications.

Dr. Liu is a member in Swedish Standard Committee on Electrical Machines.

Stefan Lundberg (Member, IEEE) received the Ph.D. degree in electrical engineering from Chalmers University of Technology, Gothenburg, Sweden, in 2007.

He is with the Division of Electric Power Engineering, Chalmers University of Technology. His main area of interest focuses on control and modeling of wind parks.